Characterization of the antimicrobial activity of the cell-penetrating peptide TAT-RasGAP$_{317-326}$

Maria Georgieva[2,&], Tytti Heinonen[1,&], Alessandra Vitale[3], Simone Hargraves[1], Senka Causevic[1], Trestan Pillonel[1], Leo Eberl[3], Christian Widmann[2,#], Nicolas Jacquier[1,#,*]

1. Institute of Microbiology, Lausanne University Hospital and University of Lausanne, Switzerland
2. Department of Biomedical Sciences, University of Lausanne, Switzerland
3. Department of Plant and Microbial Biology, University of Zurich, Switzerland

[&] These authors contributed equally to this work

[#] These authors share senior authorship

Running title: Study of TAT-RasGAP$_{317-326}$ antimicrobial activity

Keywords: Antimicrobial peptide, anticancer peptide, antibiotic resistance, TAT-RasGAP$_{317-326}$, *Escherichia coli*, *Pseudomonas aeruginosa*

*Corresponding author:

Dr. Nicolas Jacquier, Institute of Microbiology, Department of Pathology and Laboratory Medicine, CHUV, Bugnon 48, CH-1011 Lausanne, Switzerland

Phone: +41213148539 ; Fax: +41213144060 ; Email : nicolas.jacquier@chuv.ch

Abstract

The efficiency of classical antibiotics is undermined by the emergence of resistance. Antimicrobial peptides (AMPs) may represent an alternative to antibiotics currently used in the clinic. TAT-RasGAP$_{317-326}$ is one of such AMP. It is a cell-penetrating peptide with broad antimicrobial activity against Gram-positive and Gram-negative bacteria. However, the mechanisms allowing this peptide to kill bacteria are not characterized. Here, we aim to provide a better understanding of the factors influencing TAT-RasGAP$_{317-326}$ antimicrobial activity.

In this article, we show that divalent cations, serum proteins, and low pH levels modulate TAT-RasGAP$_{317-326}$ activity against bacteria. We demonstrate that low pH and divalent cations reduce the binding of the peptide to bacteria. Using transcriptomics and screening of bacterial mutant libraries, we mapped the transcriptional response of TAT-RasGAP$_{317-326}$-exposed bacteria and highlighted cellular pathways that may play a role in bacterial resistance to this peptide. We tested combinations of TAT-RasGAP$_{317-326}$ with other AMPs and detected an inhibitory effect of melittin on TAT-RasGAP$_{317-326}$ activity. Finally, we performed a resistance selection screen that revealed differences between bacterial strains with respect to their rate of resistance emergence against TAT-RasGAP$_{317-326}$.

Our study provides the first investigation of factors that impact the antimicrobial activity of TAT-RasGAP$_{317-326}$ and brings insights into the mechanisms underlying the peptide's activity.

Importance

Antibiotic resistance is an increasing concern for modern medicine. Resistant bacteria cause life-threatening infections that are very challenging to treat. Antimicrobial peptides (AMPs) could be a promising alternative to classical antibiotics because of their antibacterial properties and low propensity for the development of bacterial resistance. To maximize the efficiency of AMPs and avoid the emergence of resistance, it is important to understand the factors affecting their activity. In this study, we investigate the antimicrobial activity of a recently described AMP, TAT-RasGAP$_{317\text{-}326}$. We outline a subset of extracellular factors that influence its antimicrobial activity and characterize the bacterial response to this AMP. Our findings here also provide vital insight into the potential of bacteria developing resistance to this TAT-RasGAP$_{317\text{-}326}$ peptide. Overall, this study provides important insight into the basic mechanism of action of TAT-RasGAP$_{317\text{-}326}$ and a better understanding of the interaction between TAT-RasGAP$_{317\text{-}326}$ and its bacterial targets.

Introduction

The spread of antibiotic resistance in many bacterial species is severely limiting the benefits of antibiotics and a growing number of infections are becoming harder to treat (1). The issue is further compounded by the shortage of new classes of antibiotics that could potentially compensate for the expanding resistance to standard antibiotics. Therefore, there is a need for the development of new antimicrobials that could be used in the clinic to treat bacterial infections. Antimicrobial peptides (AMPs), several of which are already in clinical trials with promising results, represent attractive antibiotic alternatives (2).

AMPs were first described as naturally occurring peptides produced by many different organisms (2). In bacteria, AMP generation confers an advantage to the producing strain for the colonization of ecological niches (3). In multicellular organisms, AMPs such as the human cathelicidin LL-37 and bovine bactenecin, are part of the innate immune system (4). Thousands of AMPs have been described (5). Their diversity, their relatively simple structure,

and the possibility to bioengineer them, for example to increase their resistance in the gastrointestinal tract after oral administration (6), are factors that may facilitate the identification of broad spectrum AMPs targeting both Gram-positive and Gram–negative bacteria (2).

Despite their diversity, AMPs share a number of common features. They are usually short, consisting of 10-50 amino acids, display an overall positive charge and are rich in cationic and hydrophobic amino acids. While the mechanisms of action (MOA) of AMPs against pathogens vary depending on the peptide investigated, their antimicrobial activity seems to rely on electrostatic interactions between the positively charged peptide and the negatively charged bacterial surface. This interaction promotes the accumulation of AMPs at the bacterial surface where they initiate their antimicrobial activity. For example, melittin, isolated from bee venom (7), and LL-37, stored in the lysosomes of macrophages (8), have been shown to disrupt bacterial membrane integrity and cause pore formation (2). Another AMP, the circularized polypeptide polymyxin B, derived from the Gram-positive bacterium *Bacillus polymyxa*, is also positively charged and able to permeabilize bacterial membranes (9).

We recently reported antimicrobial activities for TAT-RasGAP$_{317\text{-}326}$, a cell-penetrating peptide of 22 amino acids. This peptide can kill a broad spectrum of both Gram-positive and Gram-negative bacteria *in vitro* (10). TAT-RasGAP$_{317\text{-}326}$ was initially identified as an anticancer compound that can sensitize cancer cells to genotoxins (11, 12) and to radiotherapy (13). This peptide inhibits cell migration and invasion (14) that translates into anti-metastatic activity *in vivo* (15). It can also directly lyse a subset of cancer cells by targeting plasma membrane inner leaflet-enriched phospholipids (16) in a manner that does not involve known programmed cell death pathways (17, 18). The WXW motif within the peptide sequence is required for both the anticancer and antimicrobial activities of TAT-RasGAP$_{317\text{-}326}$ (10, 19). However, we still lack a comprehensive understanding of the mechanisms behind TAT-RasGAP$_{317\text{-}326}$ antimicrobial effects.

Despite its potent *in vitro* antimicrobial activity, TAT-RasGAP$_{317\text{-}326}$ showed limited *in vivo* activity in a mouse model of *Escherichia coli* (*E. coli*) induced peritonitis (10). This could be

due to environmental factors, such as binding to serum proteins, presence of chemicals or pH variations on the activity of TAT-RasGAP$_{317-326}$, as reported for other AMPs (20). The poor biodistribution and rapid clearance of TAT-RasGAP$_{317-326}$ also contributes to its suboptimal efficacy *in vivo* (18). A better understanding of the MOA of TAT-RasGAP$_{317-326}$ and of the factors influencing its activity would aid developing strategies to improve its activity and *in vivo* applicability.

The possibility of emergence of resistance has to be considered for any antimicrobial drugs with potential clinical application. While resistance to AMPs seems to develop at a lower rate than resistance to classical antibiotics, this process is more common than previously hypothesized (21-23), indicating that a careful evaluation of factors favoring resistance towards AMPs is required to define the conditions that allow safe usage of these compounds.

In this report, we studied various parameters that could modulate the ability of TAT-RasGAP$_{317-326}$ to efficiently kill bacteria. We first determined the effect of culture medium composition and pH levels on the peptide's activity. We then performed RNA sequencing (RNA-Seq) to investigate the transcriptional response of *E. coli* incubated with TAT-RasGAP$_{317-326}$. Furthermore, we assessed which pathways are required for the peptide's activity by performing screenings of an *E. coli* single gene deletion mutants library (the Keio collection) and of a *Pseudomonas aeruginosa* PA14 (*P. aeruginosa*) transposon mutant library. Finally, we investigated the antimicrobial effect of combinations of TAT-RasGAP$_{317-326}$ with other AMPs and attempted to select resistance towards TAT-RasGAP$_{317-326}$ in several bacterial species.

Results

Divalent cations in culture medium modulate bacterial resistance to TAT-RasGAP$_{317-326}$

P. aeruginosa grown under low Mg^{2+} conditions are resistant to EDTA, gentamicin and polymyxin B via a mechanism that involves outer membrane modification (24-26). To assess whether TAT-RasGAP$_{317-326}$ antimicrobial activity is also affected by Mg^{2+} levels in culture medium, we tested the activity of the peptide in media containing different Mg^{2+} levels against two laboratory strains, *E. coli* MG1655 and *P. aeruginosa* PA14. The minimal inhibitory concentration (MIC) of TAT-RasGAP$_{317-326}$ in standard LB medium for *E. coli* and *P. aeruginosa* was determined to be 8 µM and 32 µM respectively (Table 1 and Fig. S1A-B). We observed no substantial difference in peptide MIC levels between LB and BM2-glucose minimal medium supplemented with 2 mM $MgSO_4$ (BM2 Mg^{high}) for both *E. coli* and *P. aeruginosa* (Fig. S1C-D). However, these two bacterial species displayed increased susceptibility to TAT-RasGAP$_{317-326}$ in BM2 containing 20 µM $MgSO_4$ (BM2 Mg^{low}) relative to BM2 Mg^{high} (Fig. S1E-F). Low magnesium concentrations in media, in contrast, did not sensitize bacteria to polymyxin B (Fig. S2). Actually, in the case of *P. aeruginosa*, BM2 Mg^{low} rather increased resistance to polymyxin B. This result agrees with earlier data on the connection between Mg^{2+} levels and polymyxin B resistance (24, 25). The different impact of Mg^{2+} concentrations towards polymyxin B and TAT-RasGAP$_{317-326}$ susceptibility in bacteria suggests that the mechanisms regulating susceptibility to these two AMPs are different.

BM2 is a simplified bacteriological medium. We next investigated whether Mg^{2+} also affects the sensitivity to TAT-RasGAP$_{317-326}$ in nutritionally rich medium such as Luria-Bertani (LB) medium. We found that high magnesium concentrations in LB also augmented the resistance of *E. coli* and *P. aeruginosa* to the peptide (Table 1, Fig. S1G-H and Fig. 1A-B). We therefore conclude that high Mg^{2+} levels increase bacterial resistance to TAT-RasGAP$_{317-326}$ regardless of medium composition.

Would cations other than Mg^{2+} also render bacteria more resistant to TAT-RasGAP$_{317-326}$? Addition of Fe^{2+} and Ca^{2+} increased the resistance of *E. coli* to the peptide (Fig. 1C-D). We

also found that high Mg^{2+} concentrations promoted bacterial resistance to TAT-RasGAP$_{317-326}$ both in the context of sulfate and chloride counterions (Fig. 1B and E). In contrast, ammonium sulfate did not affect bacterial susceptibility to TAT-RasGAP$_{317-326}$ (Fig. 1F). Collectively, these results indicate that the Fe^{2+}, Ca^{2+} and Mg^{2+} divalent cations hamper the ability of TAT-RasGAP$_{317-326}$ to kill bacteria.

Since divalent cations are known to influence outer membrane characteristics, we questioned whether TAT-RasGAP$_{317-326}$ binding and internalization was affected by these cations. Fe^{2+}, and to a lower extent Ca^{2+} and Mg^{2+}, inhibited binding of TAT-RasGAP$_{317-326}$ to *E. coli* and consequently the amount of peptide the bacteria would take up (Fig. 1G). This suggests that divalent cations promote bacterial resistance via a mechanism that restricts peptide binding to, and entry in bacteria.

pH levels and presence of buffering compounds affect TAT-RasGAP$_{317-326}$ antimicrobial activity

To determine whether pH of the culture medium affects the antimicrobial activity of TAT-RasGAP$_{317-326}$, we used the buffering compound 2-(N-morpholino)ethanesulfonic acid (MES) to prepare LB media with varying pH levels (from 5.5 to 7.0) (27). In the presence of MES, the pH remained stable over the course of the experiment (Table S1). Decreasing the pH in MES-containing medium inhibited the antimicrobial activity of the peptide (Fig. 2A-D and S3A-D). Note that MES by itself negatively impacted the ability of the peptide to kill bacteria (Fig. 2D-E and S3D-E), possibly due to sequestration of TAT-RasGAP$_{317-326}$ by MES following interaction of the latter's negatively charged sulfonyl hydroxide group with the cationic amino acids of the peptide. Effect of low pH on peptide activity was not due to peptide degradation as pre-incubation of the peptide at pH 5.5 did not decrease its ability to kill *E. coli* and *P. aeruginosa* when tested at pH 7 (Fig. S4A). However, the decreased killing activity of the peptide observed at low pH can be explained, similarly to what was proposed above for divalent cations, by inhibition of peptide binding to, and uptake in bacteria (Fig. 2F and Fig. S4B).

In contrast to what was seen for TAT-RasGAP$_{317-326}$, MES did not alter the ability of polymyxin B to kill *E. coli* and *P. aeruginosa* (Fig. S5, compare middle and lower graphs). Nevertheless, as was the case for TAT-RasGAP$_{317-326}$, pH reduction increased the resistance of bacteria to polymyxin B (Fig. S5, compare top and middle graphs).

Effect of serum and albumin on the antimicrobial activity of TAT-RasGAP$_{317-326}$

Serum albumin can bind to AMPs and thus lower their activity *in vivo*, causing 8-10 times increase of MIC (28, 29). Figure S6 shows that the growth inhibition activity of TAT-RasGAP$_{317-326}$ on *E. coli* was decreased by bovine serum albumin (BSA) and fetal calf serum (FCS) by 2- to 4-fold. As for other AMPs, the antibacterial activity of TAT-RasGAP$_{317-326}$ is therefore also negatively impacted by serum proteins, presumably because the peptide binds these proteins. In this context, it is worth noting that albumin is negatively charged at pH = 7 (isoelectric point of 4.7) and as such has the potential to sequester cationic peptides.

TAT-RasGAP$_{317-326}$ is bactericidal against *E. coli* and *P. aeruginosa*

To quantitate the number of culturable bacteria after incubation with TAT-RasGAP$_{317-326}$, we performed survival curves of bacteria exposed to peptide and counted colony-forming units (CFU). For *E. coli* grown in LB, 10 μM of the peptide induced an initial 2-5 fold decrease in the number of surviving bacteria but there was no further decrease upon longer incubation times (Fig. 3A), which is consistent with the observation that 10 μM is the concentration corresponding approximatively to the MIC determined by OD_{590} measurement. A more pronounced decrease in bacterial viability was observed at peptide concentrations higher than or equal to 15 μM, indicating that the peptide is bactericidal at these concentrations (Fig. 3A). We performed a similar experiment with *P. aeruginosa* in BM2 Mg^{low} medium where we observed growth inhibition at 1 μM and 2 μM TAT-RasGAP$_{317-326}$, and strong decreased bacterial viability at 5 μM and 10 μM (Fig. 3B). Interestingly, TAT-RasGAP$_{317-326}$ displayed much slower time-kill kinetics against *E. coli* than polymyxin B that is known to induce

membrane permeabilization (30) (Fig. 3C). However, difference was less visible in *P. aeruginosa* (Fig. 3D). We determined that killing of *E. coli* by TAT-RasGAP$_{317-326}$ was associated with accumulation of the peptide in the cytosol (Fig. 3E) and by changes in bacterial morphology (Fig. 3F).

TAT-RasGAP$_{317-326}$ alters the transcriptional landscape of *E. coli*

AMPs can target more than one cellular process (31). To assess the overall effect of TAT-RasGAP$_{317-326}$ on the *E. coli* transcriptome, we performed RNA-Seq analysis and compared the transcriptional profiles of bacteria exposed or not to TAT-RasGAP$_{317-326}$. For these experiments, we used 10 μM of the peptide, a concentration that inhibits growth (Fig. 3A). Among the 4419 transcripts predicted from the *E. coli* MG1655 genome, 95.6% (n = 4223) were detected in at least one condition. Figure 4A and Dataset 1 present the fold change in gene expression between bacteria incubated with and without TAT-RasGAP$_{317-326}$ as well as the average level of expression for each gene. We excluded from our analysis genes whose expression was below the threshold set at 16 reads per kilobase of transcripts per million reads (RPKM). Overall, TAT-RasGAP$_{317-326}$ treatment notably affected the expression of 962 genes (fold change > 4): 11.0% of detected genes were upregulated (red dots in Fig. 4A, Table S2) while 11.8% were downregulated (blue dots in Fig. 4A, Table S3).

We assessed and validated twelve genes from the RNA-Seq data by qRT-PCR on RNA extracted under the same conditions as for the RNA-Seq analyses. Five of these (*lpxL*, *fabF*, *marA*, *entB* and *fepA*, depicted in red in Fig. 4B) were reported by RNA-Seq as upregulated, five as downregulated (*bssR*, *frdA*, *ompF*, *nuoE* and *sdhC*, depicted in blue in Fig. 4B) and two as unchanged according to the RNA-seq analysis (*tolC* and *ompR*). One of the unchanged genes, *ompR*, was used as the housekeeping reference gene for normalization. We obtained good correlation between the fold changes obtained with RNA-Seq and with qRT-PCR, confirming the validity of the RNA-Seq data (Fig. 4B).

To determine which biological processes or pathways were over-represented among differentially expressed genes, we performed KEGG pathway (32-34) and GO term analyses

(35, 36). The analysis of KEGG pathways revealed that several metabolic and information-processing pathways were enriched among differentially expressed genes (Fig. 4C-D). For example, seven of the eight genes responsible for enterobactin synthesis in *E. coli* (included in "biosynthesis of siderophore group nonribosomal peptides" KEGG pathway) were upregulated upon peptide treatment. Other metabolic pathways such as carbon metabolism (citrate cycle, pyruvate metabolism) and oxidative phosphorylation were downregulated. GO term analysis also highlights the metabolic changes induced by TAT-RasGAP$_{317\text{-}326}$ (Fig. S7). Functions related to stress response were activated, possibly explaining the strong modifications of the transcription profiles of transporters and regulatory pathways that was observed.

Screening of the Keio *E. coli* deletion mutant library uncovers genes that regulate bacterial resistance to TAT-RasGAP$_{317\text{-}326}$

We screened the Keio collection of *E. coli* deletion mutants (37) for genes that play a role in resistance to TAT-RasGAP$_{317\text{-}326}$. Each strain of the Keio collection was grown in presence of 5 μM TAT-RasGAP$_{317\text{-}326}$. This concentration of peptide does not kill wild-type *E. coli* over a 24 hour time period following peptide addition (Fig. 3A). OD_{590} was measured 1.5, 3, 6 and 24 hours after addition of TAT-RasGAP$_{317\text{-}326}$ for each mutant in the collection (Detailed results are available in Dataset 2). We calculated the distribution of the fold change in bacterial growth upon incubation with TAT-RasGAP$_{317\text{-}326}$ versus without peptide treatment for each strain at 6 hours and 24 hours (Fig. 5A-B). Resistant strains were defined as those growing more than the wild-type average plus two times the standard deviation at 6 hours (Fig. 5A). Hypersensitive strains were defined as growing less than the wild-type average minus three times the standard deviation 24 hours after addition of the peptide (Fig. 5B). Using these thresholds, we selected 27 resistant (Table S4) and 356 hypersensitive strains (Table S5). While the wild-type strains grew slower in the presence than in the absence of TAT-RasGAP$_{317\text{-}326}$, resistant strains grew similarly in both conditions and hypersensitive strains showed no growth in the presence of the peptide (Fig. 5C). KEGG pathway analysis of the

screening results indicates that deletions of genes involved in carbon metabolism, citrate cycle and oxidative phosphorylation sensitized bacteria to TAT-RasGAP$_{317-326}$ peptide (Fig. 5D). We also found that some two-component systems and transcriptional regulators are required to maintain a normal peptide resistance rate (Fig. 5D-E). Analysis of resistant mutants showed that they carry deletions in genes involved in LPS biogenesis and oxidative phosphorylation (Table S4).

Transposon screening in *P. aeruginosa*

Since TAT-RasGAP$_{317-326}$ is active against both *E. coli* and *P. aeruginosa*, we investigated whether some of the pathways that play a role in peptide resistance are shared between the two bacterial species. We thus exposed a *P. aeruginosa* transposon mutant library (38) to TAT-RasGAP$_{317-326}$ and identified mutants that showed hypersensitivity to the peptide. We grew this library in presence or absence of 0.5 μM TAT-RasGAP$_{317-326}$ for 12 generations and performed deep sequencing in order to identify genes required for growth in the presence of the peptide (Dataset 3). We defined lack of proliferation of these mutants as a read-out of hypersensitivity to TAT-RasGAP$_{317-326}$. We identified 75 genes, whose disruption via transposon insertion caused increased sensitivity to the peptide (Table S6). Interestingly, 26 of these (35%) are associated with hypersensitivity to other antimicrobial peptides (38). Some of these genes code for LPS modifying enzymes such as ArnA, ArnB and ArnT, and for two-component regulators such as ParS and ParR that are involved in the regulation of LPS modifications (39). Among the genes, in which transposon insertion caused hypersensitivity towards TAT-RasGAP$_{317-326}$ and not towards other AMPs, we identified *algJ*, *algK* and *algX*, genes of the biosynthesis pathway of the extracellular polysaccharide alginate. We also observed that mutants in genes coding for the RND efflux transporter MdtABC and CusC, a component of the trans-periplasmic Cu^{2+} transporter CusCFBA, are hypersensitive to TAT-RasGAP$_{317-326}$. Other pathways that seem to be important for TAT-RasGAP$_{317-326}$ resistance are related to carbon metabolism, redox reactions and translation regulation (Table S6).

We next compared the lists of hypersensitive strains found in screenings in *E. coli* and in *P. aeruginosa*. We identified 15 gene orthologues, whose disruption causes hypersensitivity to the TAT-RasGAP$_{317-326}$ peptide in both *E. coli* and *P. aeruginosa* (Table 2). Among them, five are coding for two-component system proteins: *parR* and *parS* (*rtsA* and *rstB* in *E. coli*), *phoP*, *pmrB* (*qseC* in *E. coli*) and *colR* (*cusR* in *E. coli*). These five mutants display hypersensitivity to polymyxin B in *P. aeruginosa* (38), indicating that these regulatory pathways may be required for a general adaptation to AMPs. We also found genes conserved between *P. aeruginosa* and *E. coli* that respond specifically to treatment with TAT-RasGAP$_{317-326}$ and are involved in diverse cellular processes such as transcriptional regulation, DNA repair, glyoxylate detoxification, redox reactions, transmembrane transport and LPS biosynthesis (Table 2).

Effect of combining TAT-RasGAP$_{317-326}$ with other AMPs

To determine whether TAT-RasGAP$_{317-326}$ activity is affected by other AMPs, we performed growth tests of *E. coli* in presence of different combinations of TAT-RasGAP$_{317-326}$, melittin, LL-37 and polymyxin B, using sub-inhibitory concentrations of each peptide (Fig. 6A). Sub-inhibitory concentrations were chosen so that addition of two times this concentration would cause a visible drop in bacterial proliferation (Fig. 6A vs 6B). The effect of combinations of these AMPs was then tested by measuring the growth of *E. coli* in presence of combinations of any two AMPs (Fig. S8). We calculated the percentage of growth after 6 h of treatment compared to untreated control (Fig. 6C). We did not observe an increase in the effect of TAT-RasGAP$_{317-326}$ when combined with the three other AMPs tested. However, the combination of melittin and polymyxin B (2.8% of growth) and the combination of LL-37 and polymyxin B (0.8% of growth) showed increased activity. Notably, the combination of melittin and polymyxin B caused stronger growth inhibition (>95%) than obtained by doubling the concentrations of a given compound (~25% and ~40% growth inhibition for melittin and polymyxin B, respectively; Fig. 6C). This effect is reminiscent of the synergism previously reported between melittin and antibiotics such as doripenem and ceftazidime (40). In contrast, the combination of melittin

and TAT-RasGAP$_{317-326}$ showed a weaker effect than individual treatments, since sub-inhibitory concentration of melittin blocked the growth inhibition caused by the TAT-RasGAP$_{317-326}$ peptide (Fig. 6D). To better understand the cause of this effect, we performed FACS analysis using FITC-labelled TAT-RasGAP$_{317-326}$. We found that, in presence of melittin, binding of FITC-labelled TAT-RasGAP$_{317-326}$ to *E. coli* bacteria was not decreased, but apparently slightly increased when compared to the control condition where bacteria were incubated with FITC-labelled TAT-RasGAP$_{317-326}$ alone. However, we observe an apparent lower intracellular accumulation of the labelled version of TAT-RasGAP$_{317-326}$ peptide in presence of melittin (Fig. 6E).

Appearance of TAT-RasGAP$_{317-326}$ peptide-resistant strains

One argument for the introduction of AMPs in the clinic as antibiotic alternative is the low rate of associated resistance and low rates of cross-resistance to other AMPs or antibiotics (41-43). To determine if this is also the case for TAT-RasGAP$_{317-326}$, we tested the kinetics of resistance towards TAT-RasGAP$_{317-326}$ peptide in several bacterial strains (*E. coli*, *P. aeruginosa*, *S. aureus* and *S. capitis*). First, we grew the parental bacterial strains overnight in presence of sub-inhibitory concentrations of the peptide. We then diluted this parent culture into two subcultures, one of which was exposed to an increased concentration of the TAT-RasGAP$_{317-326}$ while the other was kept in the same concentration of peptide as the parent culture. Once bacterial growth was detected in the culture exposed to an elevated concentration of the peptide, the process was repeated, thereby exposing the bacterial culture to sequentially increasing concentrations of peptide for a total of 20 passages. For each passage, we measured the corresponding MIC (Fig. 7). Using this approach, we obtained strains with increased MICs for *E. coli*, *S. capitis* and *S. aureus*, but not *P. aeruginosa* (Fig. 7, Table 3 and Tables S7-10). It should be noted that the parental strain of *S. aureus* has a peptide MIC in the range 64-128 μM and this MIC rapidly increased to 256 μM (Table S10). We did not expose bacteria to higher concentrations, as the peptide started to precipitate in these conditions. To test whether the strains recovered at passage 20 for *E. coli* and passage

12 for *S. aureus* showed increased resistance to other AMPs as well, we determined the fold change of the MICs for polymyxin B, melittin and LL-37 relative to the corresponding parental strains that did not undergo selection (Table 3). Interestingly, the resistant *E. coli* strain did not show increased MICs to the other AMPs we tested as compared to the parental strain. In contrast, the other bacterial species (*P. aeruginosa*, *S. aureus*, and *S. capitis*) selected for resistance to TAT-RasGAP$_{317\text{-}326}$ showed increased MIC towards other AMPs (Table 3). Taken together, these results further indicate that application of AMPs in the clinic should be undertaken with caution, since selection of resistance is possible.

Discussion

The activity of AMPs can be influenced by external factors such as pH level, salt concentration and presence of serum components like albumin (20). Here, we assessed the effect of these factors on the antimicrobial activity of TAT-RasGAP$_{317-326}$.

Addition of divalent cations in LB medium resulted in increased bacterial resistance to TAT-RasGAP$_{317-326}$ peptide and reduced peptide binding and entry to bacteria. The mechanism contributing to lower peptide binding might be due to competition between the excess of positively charged ions in the culture medium and the cationic TAT-RasGAP$_{317-326}$ peptide for the negatively charged bacterial surface. Moreover, divalent cations are important for membrane stability, possibly influencing binding and entry of TAT-RasGAP$_{317-326}$ (44).

Similarly to divalent cations, low pH decreased peptide binding and entry. In contrast, other AMPs had increased peptide activity at low pH possibly because cationic peptides become more positively charged at low pH relative to higher pH levels, contributing to higher peptide affinity for the bacterial surface (45, 46). Because TAT-RasGAP$_{317-326}$ charge is predicted to be stable (+8) between pH 5.0 and pH 7.0 (Peptide Property Calculator, biosyn.com), it is unlikely that peptide charge contributes to the changes in peptide activity at pH 5.5. Alternatively, we hypothesize that the higher number of positively charged protons at pH 5.5 relative to pH 7.0 compete with the positively charged peptide for the anionic bacterial surface.

Using RNA-Seq experiment, we found that genes involved in carbon metabolism were downregulated upon treatment with TAT-RasGAP$_{317-326}$ (Fig. 4). Moreover, deletion or transposon mutants of genes involved in carbon metabolism and ATP production were more sensitive towards TAT-RasGAP$_{317-326}$ (Fig. 5), indicating that energy production pathways may be important for resistance towards this peptide. Adaptation to environmental stimuli might also be of importance for survival to TAT-RasGAP$_{317-326}$, since mutants lacking genes coding for some two-component systems show increased sensitivity towards TAT-RasGAP$_{317-326}$.

Another pathway that may be involved in sensitivity to TAT-RasGAP$_{317-326}$ is the LPS biosynthesis pathway. Indeed mutations affecting this pathway can cause either moderate

resistance or hypersensitivity to the peptide (Fig. 5). Deletion of *waaP* (*rfaP*), *waaQ* (*rfaQ*) or *waaY* (*rfaY*) induced resistance to the peptide possibly via changes in LPS structure or charge (47) that might alter the binding affinity of TAT-RasGAP$_{317-326}$ to LPS. In contrast, strains lacking *arnT* or *cpsB* (*wbpW* for *P. aeruginosa*) are hypersensitive to the peptide, possibly because of an inability to trigger the LPS modifications required to establish resistance towards AMPs (48, 49).

In general, activity of TAT-RasGAP$_{317-326}$ was not influenced by other AMPs. However, melittin had an inhibitory effect on TAT-RasGAP$_{317-326}$ activity, blocking its entry in bacteria (Fig. 6D-E). This rather peculiar effect might be explained by the hypothesized MOA of melittin (i.e. carpet model), in which melittin first interacts with the bacterial surface, before reaching a concentration threshold causing disruption of the bacterial membrane (50). Sub-inhibitory concentrations of melittin might thus block binding of TAT-RasGAP$_{317-326}$ to the bacterial membrane.

In summary, the results presented in this article bring a better understanding of the antimicrobial activity of TAT-RasGAP$_{317-326}$ peptide. We describe the effect of diverse factors such as salts, pH and serum proteins on the antimicrobial activity of the peptide. Furthermore, we report the effect of TAT-RasGAP$_{317-326}$ on the transcriptional landscape of *E. coli* and highlight pathways that are important for resistance of bacteria towards this AMP. We finally investigated the effect of other AMPs on the activity of TAT-RasGAP$_{317-326}$ and could select bacteria showing resistance towards TAT-RasGAP$_{317-326}$, giving important information in the perspective of a clinical use of this peptide, in order to improve its activity and to avoid rapid emergence of resistance.

Material and methods

Strains and growth conditions

E. coli strains K-12 MG1655 substrain or BW25113 were grown in LB or Basal Medium 2 (BM2; 62 mM potassium phosphate buffer [pH 7.0], 7 mM $(NH_4)_2SO_4$, 10 μM $FeSO_4$, 0.4% (wt/v) glucose and 0.5% tryptone) with high (2 mM) or low (20 μM) concentration of magnesium ($MgSO_4$) (51). *Pseudomonas aeruginosa* strain PA14 was grown either in LB or BM2 medium. *Staphylococcus capitis* (10) and *S. aureus* (ATCC 29213) strains were grown in tryptic soy broth (TSB) (52). All strains were stored at -80°C, in their respective medium, supplemented with ~25% glycerol. When required, antibiotics were added at final concentrations of 50 μg/mL (kanamycin), 20 μg/mL (gentamycin), or 100 μg/mL (carbenicillin). When indicated, LB was buffered with 100 mM of the buffering agent 2-(N-morpholino)ethanesulfonic acid (MES, Sigma-Aldrich, Saint-Louis, MO) and pH was adjusted with HCl (27). The retro-inverse TAT-RasGAP$_{317-326}$ peptide (amino acid sequence DTRLNTVWMWGGRRRQRRKKRG) and the N-terminal FITC-labelled version of this peptide were synthesized by SBS Genetech (Beijing, China) and stored at -20°C. Chemicals were purchased from Sigma-Aldrich, unless otherwise specified.

MIC measurements

The minimum inhibitory concentration (MIC) of peptide was defined as the lowest concentration of peptide that resulted in no visible growth. Overnight cultures were diluted to OD_{600} = 0.1 and grown with shaking at 37°C for 1 hour. MICs were measured by diluting these cultures (1:20 for LB and TSB cultures and 1:8 for BM2 cultures) and then adding these dilutions to 2-fold sequential dilutions of the peptide in 96-well plates. Volume of media (with peptide) per well was 100 μl and 10 μl of diluted cultures were added to each well. Cell growth was monitored via OD_{590} measurement after overnight growth with shaking at 37°C. OD_{590} readings were measured by FLUOstar Omega microplate reader (BMG Labtech, Ortenberg, Germany). Peptide-free growth control wells and bacteria-free contamination control wells

were included. First concentration at which no bacterial growth could be detected was defined as the MIC.

Growth curves

Overnight cultures were diluted to OD_{600} = 0.1 and grown with shaking at 37°C for 1 hour, before addition of peptide. Cell growth was monitored via OD_{600} measurement by Novaspec II Visible spectrophotometer (Pharmacia LKB Biotechnology, Cambridge, England) at 2, 4 and 6 hours.

CFU measurements

Overnight cultures were diluted to OD_{600} = 0.1 and grown with shaking at 37°C for 1 hour, before addition of the peptide. Each time point was taken by removing 10 μl and performing 10-fold serial dilutions. Dilutions of each condition were then plated in the absence of peptide and grown at 37°C overnight. CFU were measured by counting the number of colonies on the plates after overnight incubation.

Confocal microscopy

Overnight cultures of *E. coli* MG1655 were diluted to OD_{600} = 0.1, grown for 1 hour, incubated for 1 hour with 10 μM FITC-labelled TAT-$RasGAP_{317-326}$, stained with 5 μg/ml FM4-64 and fixed with 4% paraformaldehyde solution. Incubation with DAPI was subsequently performed and pictures were acquired on a LSM710 confocal microscope (Zeiss, Oberkochen, Germany). Images were analyzed with ImageJ software (53).

Electron microscopy

Bacteria were fixed with 2.5% glutaraldehyde solution (EMS, Hatfield, PA) in Phosphate Buffer (PB 0.1 M pH 7.4) for 1 hour at room temperature. Then, bacterial samples were incubated in a freshly prepared mix of 1% osmium tetroxide (EMS) and 1.5% potassium

ferrocyanide in phosphate buffer for 1 hour at room temperature. The samples were then washed three times in distilled water and spun down in 2% low melting agarose, solidified on ice, cut into 1 mm^3 cubes and dehydrated in acetone solution at graded concentrations (30% for 40 minutes; 50% for 40 minutes; 70% for 40 minutes and 100% for 3 times 1 hour). This was followed by infiltration in Epon at graded concentrations (Epon 1/3 acetone for 2 hours; Epon 3/1 acetone for 2 hours, Epon 1/1 for 4 hours and Epon 1/1 for 12 hours) and finally polymerization for 48 hours at 60°C in a laboratory oven. Ultrathin sections of 50 nm were cut on a Leica Ultramicrotome (Leica Mikrosysteme GmbH, Vienna, Austria) and placed on a copper slot grid 2x1mm (EMS) coated with a polystyrene film. The bacterial sections were stained in 4% uranyl acetate for 10 minutes, rinsed several times with water, then incubated in Reynolds lead citrate and finally rinsed several times with water before imaging.

Micrographs (10x10 tiles) with a pixel size of 1.209 nm over an area of 40x40 µm were taken with a transmission electron microscope Philips CM100 (Thermo Fisher Scientific, Waltham, MA) at an acceleration voltage of 80kV with a TVIPS TemCam-F416 digital camera (TVIPS GmbH, Gauting, Germany). Large montage alignments were performed using Blendmont command-line program from the IMOD software (54) and treated with ImageJ software.

Flow cytometry

Overnight cultures of *E. coli* MG1655 were diluted 1:100 and grown to mid exponential phase (OD_{600} = 0.4-0.6) with shaking at 37°C. Each culture was then diluted to OD_{600} = 0.1, grown with shaking at 37°C for 1 hour and then treated with 10 µM FITC-labelled peptide for 1 hour. Following peptide treatment, bacterial cells were washed in PBS and diluted 1:5 before acquisition on a CytoFLEX benchtop flow cytometer (Beckman Coulter). For each sample, 10,000 events were collected and analyzed. Extracellular fluorescence was quenched with 0.2% Trypan Blue (TB). TB is an efficient quencher of extracellular fluorescence (55-58) and allows quantification of fluorescent signal from intracellular peptide (not subject to quenching by TB). P values were calculated using ratio paired t-test.

RNA-Seq

Overnight cultures of *E. coli* MG1655 were diluted to OD_{600} = 0.1 and grown with shaking at 37°C for one hour to mid exponential phase (OD_{600} = 0.4-0.6). Cultures were then treated with TAT-RasGAP$_{317-326}$ (10 μM) or left untreated (negative control), and grown with shaking at 37°C for an additional hour. For RNA extraction, protocol 1 in the RNAprotect Bacteria Reagent Handbook (Enzymatic lysis of bacteria) was followed using the RNeasy Plus Mini Kit (Qiagen) using TE buffer (10 mM Tris-HCl, 1 mM EDTA, pH 8.0) containing 1 mg/ml lysozyme (AppliChem, Chicago, IL). In the last step, RNA was eluted in 30 μl RNase-free water. Next, any contaminating DNA was removed using the DNA-free™ DNA Removal Kit (Invitrogen, Carlsbad, CA). 10x DNase buffer was added to the 30 μl eluted RNA with 2 μl rDNase I. This mix was incubated for 30 minutes at 37°C followed by rDNase I inactivation with 7 μl DNase Inactivation Reagent for 2 minutes with shaking (700 rpm) at room temperature. Samples were then centrifuged for 90 seconds at 10,000 x *g*, supernatant was transferred to a new tube, and stored at -80°C. Integrity of the samples was verified using the Standard Sensitivity RNA Analysis kit (Advanced Analytical, Ankeny, IA) with the Fragment Analyser Automated CE System (Labgene Scientific, Châtel-Saint-Denis, Switzerland). Samples that met RNA-Seq requirements were further processed and sent for sequencing. Preparation of the libraries and Illumina HiSeq platform (1x50 bp) sequencing were performed by Fasteris (Plan-les-Ouates, Switzerland). Raw reads were trimmed with trimmomatic version 0.36 (59) (parameters: ILLUMINACLIP: NexteraPE-PE.fa:3:25:6, LEADING: 28, TRAILING: 28 MINLEN: 30). Trimmed reads were mapped to the genome of *E. coli* K-12 MG1655 (accession: NC_000913.3) with bwa mem version 0.7.17 (https://arxiv.org/abs/1303.3997) using default parameters. Htseq version 0.11.2 (60) was used to count reads aligned to each gene (parameters: --stranded=no -t gene). Normalized expression values were calculated as Reads Per Kilobase of transcript per Million mapped reads (RPKM) with edgeR (61).

Keio collection screening

Deletion mutants from the Keio collection (37, 62) were used. Overnight cultures were diluted 1:100 in LB medium. Bacteria were incubated at 37°C with shaking for 1 hour before adding TAT-RasGAP$_{317-326}$ (5 µM final concentration). Plates were incubated statically at 37°C and OD_{590} was measured at 0 hour, 1.5 hour, 3 hours, 6 hours and 24 hours with FLUOstar Omega plate reader. Measurements were combined and analysed with R (version 3.6.1, (63)). Data analysis and visualisation were performed respectively with the *dplyr* (version 0.8.5) and *ggplot2* (version 3.3.0) packages from the *tidyverse* (version 1.3.0) environment. Since starting OD_{590} varied between strains, the corresponding starting value (T0 measurement) was subtracted at each measurement. Then, for each strain, the growth with TAT-RasGAP$_{317-326}$ was divided by the growth without peptide for normalization. The threshold for resistance was set based on normalized growth at 6 hours (NG6h) as 'NG6h strain' > 'NG6h WT + 2 x SD(NG6h WT)'. Hypersensitive strains were selected based on NG at 24 hours (NG24h) as 'NG24h strain' < 'NG24h WT – 3 x SD (NG24h WT)'.

Gene ontology (GO) annotation (36) was obtained from GO database (2020-09-01, "http://current.geneontology.org/annotations") and assigned to the list of gene deletion inducing hypersensitivity with the GO.db package (version 3.10.0 (64)). GO IDs were assigned to each gene and the corresponding GO names were obtained with the "Term" function. Additionally, the same set of genes was subjected to KEGG pathways analysis (32) with the KEGGREST package (version 1.26.1). Briefly, the KEGG orthology (KO) and KEGG pathway annotation were obtained from the KEGG database (34) for *E. coli* K-12 MG1655 (eco). The code is available on Github (https://github.com/njacquie/TAT-RasGAP_project).

***Pseudomonas aeruginosa* PA14 transposon library screening**

The library of transposon (Tn) mutants in *P. aeruginosa* PA14 (38) was grown in BM2 supplemented with 20 µM $MgSO_4$ (51) and 0.2% L-rhamnose monohydrate (Sigma-Aldrich) in the absence or presence of 0.5 µM TAT-RasGAP$_{317-326}$. Following growth for 12 generations, genomic DNA (gDNA) was extracted with the GenElute Bacterial Genomic DNA Kit (Sigma-

Aldrich). The transposon sequencing (Tn-seq) circle method (65, 66) was employed to sequence the transposon junctions. Briefly, the gDNA was sheared to an average size of 300 bp fragments with a focused-ultrasonicator. The DNA fragments were repaired and ligated to adapters with the NEBNext Ultra II DNA Library Prep Kit for Illumina (New England Biolabs). Following restriction of the Tn with BamHI (New England Biolabs), the fragments were circularized by ligation and exonuclease treatment was applied to remove undesired non-circularized DNAs (65). The Tn junctions were PCR amplified and amplicons were sequenced with the MiSeq Reagent Kit v2, 300-cycles (Illumina).

Following sequencing, the adapter sequences of the reads (.fastq) were trimmed with the command line “cutadapt -a adapter -q quality -o output.fastq.gz input.fastq.gz” (67). The software Tn-Seq Explorer (68) mapped the trimmed and paired reads onto the *P. aeruginosa* UCBPP-PA14 genome (69), and determined the unique insertion density (UID, i.e. the number of unique Tn insertions divided per the length of the gene). The normalized UID between the treated and non-treated samples were compared and this ratio (log2-fold change, FC) was used to identify resistant determinants (log2-FC < - 1.0 and normalized UID > 0.0045).

Selection of resistant mutants

Bacteria were grown in the corresponding medium, diluted 1:100 and cultured overnight with 0.5x MIC of TAT-RasGAP$_{317-326}$. The subculture was diluted 1:100 and incubated with 0.5x or 1x MIC overnight. Cells that successfully grew were diluted 1:100 in medium containing the same concentration or twice the concentration of peptide. Each dilution in fresh medium containing peptide is considered one passage. This process was repeated for up to 20 passages.

Authorship

MG, TH, NJ, AV, SH and SC performed experiments. MG, TH, LE, CW and NJ were involved in the planning of the project and discussed the results. MG, TH, NJ and TP analysed the results. MG, CW and NJ wrote the manuscript. All the authors proofread the manuscript.

Acknowledgments

We would like to thank Sébastien Aeby for technical support, Valentin Scherz for support in bioinformatics analyses and Prof. Gilbert Greub for sharing equipment and laboratories. This study was supported by an interdisciplinary grant of the Faculty of Biology and Medicine of the University of Lausanne.

Conflicts of interest

The authors declare no conflicts of interest.

References

1. O'Neill J (2016) Tackling Drug-resistant Infections Globally: Final Report and Recommendations of the Review on Antimicrobial Resistance. ed Government H (London).
2. Kumar P, Kizhakkedathu JN, & Straus SK (2018) Antimicrobial Peptides: Diversity, Mechanism of Action and Strategies to Improve the Activity and Biocompatibility In Vivo. *Biomolecules* 8(1).
3. Hassan M, Kjos M, Nes IF, Diep DB, & Lotfipour F (2012) Natural antimicrobial peptides from bacteria: characteristics and potential applications to fight against antibiotic resistance. *J Appl Microbiol* 113(4):723-736.
4. Xhindoli D*, et al.* (2016) The human cathelicidin LL-37--A pore-forming antibacterial peptide and host-cell modulator. *Biochim Biophys Acta* 1858(3):546-566.
5. Wang G, Li X, & Wang Z (2016) APD3: the antimicrobial peptide database as a tool for research and education. *Nucleic Acids Res* 44(D1):D1087-1093.
6. Kong XD*, et al.* (2020) De novo development of proteolytically resistant therapeutic peptides for oral administration. *Nat Biomed Eng* 4(5):560-571.
7. Hong J*, et al.* (2019) How Melittin Inserts into Cell Membrane: Conformational Changes, Inter-Peptide Cooperation, and Disturbance on the Membrane. *Molecules* 24(9).
8. Mendez-Samperio P (2010) The human cathelicidin hCAP18/LL-37: a multifunctional peptide involved in mycobacterial infections. *Peptides* 31(9):1791-1798.
9. Srinivas P & Rivard K (2017) Polymyxin Resistance in Gram-negative Pathogens. *Curr Infect Dis Rep* 19(11):38.
10. Heulot M*, et al.* (2017) The Anticancer Peptide TAT-RasGAP317-326 Exerts Broad Antimicrobial Activity. *Front Microbiol* 8:994.
11. Michod D, Yang JY, Chen J, Bonny C, & Widmann C (2004) A RasGAP-derived cell permeable peptide potently enhances genotoxin-induced cytotoxicity in tumor cells. *Oncogene* 23(55):8971-8978.
12. Michod D*, et al.* (2009) Effect of RasGAP N2 fragment-derived peptide on tumor growth in mice. *J Natl Cancer Inst* 101(11):828-832.
13. Tsoutsou P*, et al.* (2017) TAT-RasGAP317-326 Enhances Radiosensitivity of Human Carcinoma Cell Lines In Vitro and In Vivo through Promotion of Delayed Mitotic Cell Death. *Radiat Res* 187(5):562-569.
14. Barras D, Lorusso G, Ruegg C, & Widmann C (2014) Inhibition of cell migration and invasion mediated by the TAT-RasGAP317-326 peptide requires the DLC1 tumor suppressor. *Oncogene* 33(44):5163-5172.
15. Barras D*, et al.* (2014) Fragment N2, a caspase-3-generated RasGAP fragment, inhibits breast cancer metastatic progression. *Int J Cancer* 135(1):242-247.
16. Serulla M*, et al.* (2020) TAT-RasGAP317-326 kills cells by targeting inner-leaflet-enriched phospholipids. *Proc Natl Acad Sci U S A*.
17. Annibaldi A, Heulot M, Martinou JC, & Widmann C (2014) TAT-RasGAP317-326-mediated tumor cell death sensitization can occur independently of Bax and Bak. *Apoptosis* 19(4):719-733.
18. Heulot M*, et al.* (2016) The TAT-RasGAP317-326 anti-cancer peptide can kill in a caspase-, apoptosis-, and necroptosis-independent manner. *Oncotarget* 7(39):64342-64359.
19. Barras D*, et al.* (2014) A WXW motif is required for the anticancer activity of the TAT-RasGAP317-326 peptide. *J Biol Chem* 289(34):23701-23711.
20. Walkenhorst WF (2016) Using adjuvants and environmental factors to modulate the activity of antimicrobial peptides. *Biochim Biophys Acta* 1858(5):926-935.
21. Perron GG, Zasloff M, & Bell G (2006) Experimental evolution of resistance to an antimicrobial peptide. *Proc Biol Sci* 273(1583):251-256.
22. Joo HS, Fu CI, & Otto M (2016) Bacterial strategies of resistance to antimicrobial peptides. *Philos Trans R Soc Lond B Biol Sci* 371(1695).
23. Blanco P, Hjort K, Martinez JL, & Andersson DI (2020) Antimicrobial Peptide Exposure Selects for Resistant and Fit Stenotrophomonas maltophilia Mutants That Show Cross-Resistance to Antibiotics. *mSphere* 5(5).
24. Macfarlane EL, Kwasnicka A, Ochs MM, & Hancock RE (1999) PhoP-PhoQ homologues in Pseudomonas aeruginosa regulate expression of the outer-membrane protein OprH and polymyxin B resistance. *Mol Microbiol* 34(2):305-316.
25. McPhee JB, Lewenza S, & Hancock RE (2003) Cationic antimicrobial peptides activate a two-component regulatory system, PmrA-PmrB, that regulates resistance to polymyxin B and cationic antimicrobial peptides in Pseudomonas aeruginosa. *Mol Microbiol* 50(1):205-217.

26. Olaitan AO, Morand S, & Rolain JM (2014) Mechanisms of polymyxin resistance: acquired and intrinsic resistance in bacteria. *Front Microbiol* 5:643.
27. Ma Z*, et al.* (2003) GadE (YhiE) activates glutamate decarboxylase-dependent acid resistance in Escherichia coli K-12. *Molecular Microbiology* 49(5):1309-1320.
28. Svenson J, Brandsdal BO, Stensen W, & Svendsen JS (2007) Albumin binding of short cationic antimicrobial micropeptides and its influence on the in vitro bactericidal effect. *J Med Chem* 50(14):3334-3339.
29. Findlay B, Zhanel GG, & Schweizer F (2012) Investigating the antimicrobial peptide 'window of activity' using cationic lipopeptides with hydrocarbon and fluorinated tails. *Int J Antimicrob Agents* 40(1):36-42.
30. Daugelavicius R, Bakiene E, & Bamford DH (2000) Stages of polymyxin B interaction with the Escherichia coli cell envelope. *Antimicrob Agents Chemother* 44(11):2969-2978.
31. Brazas MD & Hancock RE (2005) Using microarray gene signatures to elucidate mechanisms of antibiotic action and resistance. *Drug Discov Today* 10(18):1245-1252.
32. Kanehisa M & Goto S (2000) KEGG: kyoto encyclopedia of genes and genomes. *Nucleic Acids Res* 28(1):27-30.
33. Kanehisa M, Sato Y, Furumichi M, Morishima K, & Tanabe M (2019) New approach for understanding genome variations in KEGG. *Nucleic Acids Res* 47(D1):D590-D595.
34. Kanehisa M (2019) Toward understanding the origin and evolution of cellular organisms. *Protein Sci* 28(11):1947-1951.
35. Ashburner M*, et al.* (2000) Gene ontology: tool for the unification of biology. The Gene Ontology Consortium. *Nat Genet* 25(1):25-29.
36. The Gene Ontology C (2019) The Gene Ontology Resource: 20 years and still GOing strong. *Nucleic Acids Res* 47(D1):D330-D338.
37. Baba T*, et al.* (2006) Construction of Escherichia coli K-12 in-frame, single-gene knockout mutants: the Keio collection. *Mol Syst Biol* 2:2006 0008.
38. Vitale A*, et al.* (2020) Identification of Genes Required for Resistance to Peptidomimetic Antibiotics by Transposon Sequencing. *Front Microbiol* 11:1681.
39. Fernandez L*, et al.* (2010) Adaptive resistance to the "last hope" antibiotics polymyxin B and colistin in Pseudomonas aeruginosa is mediated by the novel two-component regulatory system ParR-ParS. *Antimicrob Agents Chemother* 54(8):3372-3382.
40. Akbari R*, et al.* (2019) Highly Synergistic Effects of Melittin with Conventional Antibiotics Against Multidrug-Resistant Isolates of Acinetobacter baumannii and Pseudomonas aeruginosa. *Microb Drug Resist* 25(2):193-202.
41. Lazar V*, et al.* (2018) Antibiotic-resistant bacteria show widespread collateral sensitivity to antimicrobial peptides. *Nat Microbiol* 3(6):718-731.
42. Spohn R*, et al.* (2019) Integrated evolutionary analysis reveals antimicrobial peptides with limited resistance. *Nat Commun* 10(1):4538.
43. Lazzaro BP, Zasloff M, & Rolff J (2020) Antimicrobial peptides: Application informed by evolution. *Science* 368(6490).
44. Clifton LA*, et al.* (2015) Effect of divalent cation removal on the structure of gram-negative bacterial outer membrane models. *Langmuir* 31(1):404-412.
45. Lee IH, Cho Y, & Lehrer RI (1997) Effects of pH and salinity on the antimicrobial properties of clavanins. *Infect Immun* 65(7):2898-2903.
46. Walkenhorst WF, Klein JW, Vo P, & Wimley WC (2013) pH Dependence of microbe sterilization by cationic antimicrobial peptides. *Antimicrob Agents Chemother* 57(7):3312-3320.
47. Yethon JA, Heinrichs DE, Monteiro MA, Perry MB, & Whitfield C (1998) Involvement of waaY, waaQ, and waaP in the modification of Escherichia coli lipopolysaccharide and their role in the formation of a stable outer membrane. *J Biol Chem* 273(41):26310-26316.
48. Whitfield C (2006) Biosynthesis and assembly of capsular polysaccharides in Escherichia coli. *Annu Rev Biochem* 75:39-68.
49. Yan A, Guan Z, & Raetz CR (2007) An undecaprenyl phosphate-aminoarabinose flippase required for polymyxin resistance in Escherichia coli. *J Biol Chem* 282(49):36077-36089.
50. Lee MT, Sun TL, Hung WC, & Huang HW (2013) Process of inducing pores in membranes by melittin. *Proc Natl Acad Sci U S A* 110(35):14243-14248.
51. Fernandez L*, et al.* (2012) The two-component system CprRS senses cationic peptides and triggers adaptive resistance in Pseudomonas aeruginosa independently of ParRS. *Antimicrob Agents Chemother* 56(12):6212-6222.
52. Missiakas DM & Schneewind O (2013) Growth and laboratory maintenance of Staphylococcus aureus. *Curr Protoc Microbiol* Chapter 9:Unit 9C 1.

53. Schneider CA, Rasband WS, & Eliceiri KW (2012) NIH Image to ImageJ: 25 years of image analysis. *Nat Methods* 9(7):671-675.
54. Kremer JR, Mastronarde DN, & McIntosh JR (1996) Computer visualization of three-dimensional image data using IMOD. *J Struct Biol* 116(1):71-76.
55. Sahlin S, Hed J, & Rundquist I (1983) Differentiation between attached and ingested immune complexes by a fluorescence quenching cytofluorometric assay. *J Immunol Methods* 60(1-2):115-124.
56. Loike JD & Silverstein SC (1983) A fluorescence quenching technique using trypan blue to differentiate between attached and ingested glutaraldehyde-fixed red blood cells in phagocytosing murine macrophages. *J Immunol Methods* 57(1-3):373-379.
57. Jevprasesphant R, Penny J, Attwood D, & D'Emanuele A (2004) Transport of dendrimer nanocarriers through epithelial cells via the transcellular route. *J Control Release* 97(2):259-267.
58. Wan CP, Park CS, & Lau BH (1993) A rapid and simple microfluorometric phagocytosis assay. *J Immunol Methods* 162(1):1-7.
59. Bolger AM, Lohse M, & Usadel B (2014) Trimmomatic: a flexible trimmer for Illumina sequence data. *Bioinformatics* 30(15):2114-2120.
60. Anders S, Pyl PT, & Huber W (2015) HTSeq--a Python framework to work with high-throughput sequencing data. *Bioinformatics* 31(2):166-169.
61. Robinson MD, McCarthy DJ, & Smyth GK (2010) edgeR: a Bioconductor package for differential expression analysis of digital gene expression data. *Bioinformatics* 26(1):139-140.
62. Yamamoto N*, et al.* (2009) Update on the Keio collection of Escherichia coli single-gene deletion mutants. *Mol Syst Biol* 5:335.
63. Team RC (2019) R: A language and environment for statistical computing. .
64. Carslon M (2019) GO.db: A set of annotation maps describing the entire Gene Ontology.
65. Gallagher LA, Shendure J, & Manoil C (2011) Genome-scale identification of resistance functions in Pseudomonas aeruginosa using Tn-seq. *mBio* 2(1):e00315-00310.
66. Gallagher LA*, et al.* (2013) Sequence-defined transposon mutant library of Burkholderia thailandensis. *mBio* 4(6):e00604-00613.
67. Martin M (2011) Cutadapt removes adapter sequences from high-throughput sequencing reads. *EMBnet.journal* 17:10-12.
68. Solaimanpour S, Sarmiento F, & Mrazek J (2015) Tn-seq explorer: a tool for analysis of high-throughput sequencing data of transposon mutant libraries. *PLoS One* 10(5):e0126070.
69. Winsor GL*, et al.* (2016) Enhanced annotations and features for comparing thousands of Pseudomonas genomes in the Pseudomonas genome database. *Nucleic Acids Res* 44(D1):D646-653.

Tables:

Table 1: *E. coli* MG1655 and *P. aeruginosa* PA14 sensitivity to TAT-RasGAP$_{317-326}$ varies depending on the growth medium used. *E. coli* MG1655 was grown overnight in the indicated medium, diluted to OD_{600} = 0.1 and grown for 1 hour. Culture was then diluted 20 times and 10 µl was added per well of a 96-well plate containing serial dilutions of TAT-RasGAP$_{317-326}$. OD_{590} was measured after 16 hours of incubation in presence of the indicated concentrations of TAT-RasGAP$_{317-326}$ and MIC is defined as the lowest concentration of TAT-RasGAP$_{317-326}$ that completely inhibited bacterial proliferation. IC_{50} is defined as the concentration required to inhibit 50% of growth and was calculated using GraphPad Prism 8. Indicated strains were grown overnight and diluted respectively in LB, LB with 2mM $MgSO_4$ (LB Mg^{high}), BM2 with 2mM $MgSO_4$ (BM2 Mg^{high}), or BM2 with 20 µM $MgSO_4$ (BM2 Mg^{low}).

		TAT-RasGAP$_{317-326}$	
	Medium	MIC (µM)	IC_{50} (µM)
E. coli MG1655	LB	8	3
	BM2 Mg^{high}	4	2
	BM2 Mg^{low}	0.5	0.3
	LB Mg^{high}	32	16.3
P.aeruginosa PA14	LB	32	7.2
	BM2 Mg^{high}	32	10.1
	BM2 Mg^{low}	4	1.7
	LB Mg^{high}	64	20.8

Table 2: Genes found as more sensitive in both *P. aeruginosa* by transposon library screening and in *E. coli* by Keio collection screening. List of the genes, whose disruption generated mutant strains found as sensitive in transposon library screening in *P. aeruginosa* and whose orthologues in *E. coli* were detected as sensitive in Keio collection screening. Transposon mutants of *P. aeruginosa* were incubated in presence or absence of 0.5 μM TAT-RasGAP$_{317-326}$ in BM2 Mg^{low} medium for 12 generations. Transposon junctions were amplified and sequenced. Fold change (FC) between abundance of transposon mutants with incubation in absence (BM2) or presence (TATRasGAP) of the peptide was calculated and values are presented as Log$_2$ of the FC. Inf indicates that no mutant was detected upon peptide treatment, and therefore Log$_2$ of the FC could not be calculated. Shown also are results obtained in a former study using the same transposon library that indicate which gene disruptions also cause hypersensitivity to polymyxin B (38). Ratio in Keio screening column indicates whether sensitivity was detected in both replicates of the Keio collections.

Locus_tag	Gene_symbol	Description	Category	Log$_2$(FC_BM2vsTATRasGAP)	Hypersensitivity to Polymixin B	*E. coli* homologues	Keio screening
PA14_41260	*parR*	two-component response regulator	Two-component regulator system	-4.268533546	Yes	*rstA*	Hypersensitive (2/2)
PA14_41270	*parS*	two-component sensor	Two-component regulator system	Inf	Yes	*rstB*	Hypersensitive (2/2)
PA14_49180	*phoP*	two-component response regulator PhoP	Two-component regulator system	Inf	Yes	*phoP*	Hypersensitive (2/2)
PA14_56950	*colR*	two-component response regulator	Two-component regulator system	Inf	Yes	*cusR*	More sensitive (1/2)
PA14_63160	*pmrB*	PmrB: two-component regulator system signal sensor kinase PmrB	Two-component regulator system	-3.492272393	Yes	*qseC*	Hypersensitive (2/2)
PA14_02390		transcriptional regulator	Transcription regulation	-5.436478184		*cynR*	Hypersensitive (2/2)
PA14_04160		transcriptional regulator	Transcription regulation	-1.231246313		*yjiK*	Hypersensitive (1/2)
PA14_70450	*rpoZ*	DNA-directed RNA polymerase subunit omega	Transcription regulation	-1.69421829		*rpoZ*	Hypersensitive (2/2)
PA14_65200	*rnr*	exoribonuclease RNase R	Translation regulation	-1.623618886		*rnr*	More sensitive (1/2)
PA14_18330	*arnT*	4-amino-4-deoxy-L-arabinose transferase	LPS biosynthesis	Inf	Yes	*arnT*	More sensitive (1/2)
PA14_71970	*wbpW*	GDP-mannose pyrophosphorylase	LPS biosynthesis	-4.335647742		*cpsB*	Hypersensitive (2/2)
PA14_18690		peroxidase	Oxido-reduction	-1.121328621		*ahpC*	More sensitive (1/2)
PA14_31920	*opmB*	outer membrane protein	Transmembrane transport	-5.044160761		*cusC*	More sensitive (1/2)
PA14_42700	*alkA*	DNA-3-methyladenine glycosidase II	DNA repair	-1.276606847		*alkA*	Hypersensitive (1/2)
PA14_52890		ring-cleaving dioxygenase	Antibiotic resistance	-1.036324267		*gloA*	Hypersensitive (1/2)

Table 3: MICs of TAT-RasGAP$_{317-326}$-resistant strains towards other AMPs. Fold change of MICs between the original strains (*E. coli* MG1655, *P. aeruginosa* PA14, *S. capitis* and *S. aureus* ATCC 29213) and strains exposed to increasing concentrations of TAT-RasGAP$_{317-326}$ for 20 passages. MICs were measured as described for Fig. 1. n.d.: not determined: MIC of the strain could not be determined.

	TAT-RasGAP$_{317-326}$	Polymyxin B	Melittin	LL-37
E. coli	16	0.5	0.5	0.5
P. aeruginosa	4	2	>2	n.d.
S. capitis	32	>2	2	n.d.
S. aureus	>4	n.d.	8	n.d.

Figure legends:

Figure 1. Divalent cations modulate bacterial resistance towards TAT-RasGAP$_{317\text{-}326}$.

(A-F) *E. coli* MG1655 was grown overnight at 37°C in LB supplemented with 2 mM of the indicated salt and diluted to OD_{600} = 0.1. Bacterial suspension was then grown 1 hour at 37°C before addition of the indicated concentrations of TAT-RasGAP$_{317\text{-}326}$. OD_{600} was measured at the indicated times after the initial dilution. Error bars represent standard deviation of two independent experiments. **(G)** *E. coli* MG1655 was grown overnight at 37°C in LB containing 2 mM of the indicated salts and diluted to OD_{600} = 0.1. Bacterial binding and uptake of 10 µM FITC-labelled TAT-RasGAP$_{317\text{-}326}$ was recorded in triplicate via flow cytometry with (Intracellular) or without (Total) quenching with 0.2 % trypan blue. Mean fluorescence intensities (MFI) were measured for triplicates. P values were calculated by ratio paired t-test between the indicated condition and the LB control.

Figure 2. TAT-RasGAP$_{317\text{-}326}$ activity is negatively impacted by low pH.

(A-E) *E. coli* MG1655 was grown overnight at 37°C in LB medium containing 100 mM MES at the indicated pH **(A-D)** or non-buffered LB at pH 7.0 **(E)**. Cultures were diluted to OD_{600} = 0.1 in the same medium and grown one hour at 37°C before addition of the indicated concentrations of TAT-RasGAP$_{317\text{-}326}$. OD_{600} was measured at the indicated time points. Error bars represent standard deviation of two independent experiments. **(F)** *E. coli* MG1655 was grown overnight at 37°C in LB containing or not 100 mM MES at the indicated pH, diluted to OD_{600} = 0.1 in the same medium and grown one hour at 37°C. Bacterial binding and uptake of 10 µM FITC-labelled TAT-RasGAP$_{317\text{-}326}$ was recorded in triplicate via flow cytometry with (Intracellular) or without (Total) quenching with 0.2 % trypan blue (TB). Mean fluorescence intensities (MFI) were measured for triplicates. P values were calculated using ratio paired t-test between the indicated conditions.

Figure 3. TAT-RasGAP$_{317-326}$ is bactericidal against *E. coli* and *P. aeruginosa*.

(A-B) Overnight cultures of *E. coli* MG1655 in LB (A) and *P. aeruginosa* PA14 in BM2 Mg^{low} (B) were diluted to OD_{600} = 0.1 and incubated at 37°C for 1 hour. TAT-RasGAP$_{317-326}$ was then added at the indicated concentrations. Samples were taken at the indicated time points, serially diluted 10-fold in fresh LB and plated on LB agar plates. Number of colony forming units per ml (CFU/ml) of original culture was calculated. Error bars show standard deviation for a minimum of two independent experiments. **(C)** *E. coli* cultures were treated as in (A). TAT-RasGAP$_{317-326}$ (20 µM) or polymyxin B (2.5 µg/ml) were added as indicated. Samples were taken at the indicated time points and CFU/ml were determined as in (A). Error bars show standard deviation of a minimum of two independent experiments. **(D)** *P. aeruginosa* cultures were treated as in (B). TAT-RasGAP$_{317-326}$ (10 µM) or polymyxin B (10 µg/ml) were added as indicated. Samples were taken at the indicated time points and CFU/ml were determined as in (A). Error bars show standard deviation of minimum of two independent experiments. **(E)** *E. coli* MG1655 grown overnight and diluted to OD_{600} = 0.1 was incubated for 1 hour with or without 10 µM FITC-labelled TAT-RasGAP$_{317-326}$ (Green). The bacteria were then labelled with 5 µg/ml FM4-64 (Red) and fixed with 4% paraformaldehyde solution. Incubation with DAPI (Blue) was subsequently performed. Pictures were taken with a Zeiss LSM710 confocal microscope and analyzed using ImageJ software. Bar = 2 µm. **(F)** *E. coli* bacteria treated for 1 hour with 10 µM TAT-RasGAP$_{317-326}$ were fixed using glutaraldehyde and prepared for electron microscopy as described in Material and Methods section. Samples were imaged via transmission electron microscopy. Images were analyzed using ImageJ software. Bar = 2 µm.

Figure 4. TAT-RasGAP$_{317-326}$ remodels the transcriptional landscape of *E. coli*.

RNA-seq analysis was performed on *E. coli* MG1655 incubated for 1 hour with or without 10 µM TAT-RasGAP$_{317-326}$. **(A**) MA-plot of the average gene expression (x-axis, RPKM: read per

kilobase million) vs the differential expression (y-axis). Threshold for gene expression is indicated with the blue vertical line. The red lines indicate the cut-off limit for upregulated (red dots) and downregulated (blue dots) genes. **(B)** Correlation between RNA-seq (log_2 Fold Change) and qRT-PCR (log_2 Relative Quantification) differential expression performed on RNA extracted from *E. coli* treated for one hour with or without 10 μM TAT-RasGAP$_{317-326}$ for a set of genes detected by RNA-seq as downregulated by the peptide (blue), not changed (grey) or upregulated (red). Gene expression was measured in duplicates on two independent extracted RNA sets. **(C-D)** Fraction of KEGG pathway genes that are upregulated **(C)** or downregulated **(D)** after treatment with TAT-RasGAP$_{317-326}$. Dot size indicates the number of genes in the selection.

Figure 5. Selection of hypersensitive and resistant *E. coli* deletion mutants from KEIO collection.

Deletion mutants and corresponding wild-type strain were grown in LB medium with or without 5 μM TAT-RasGAP$_{317-326}$ and OD_{590} was measured at 0, 1.5, 3, 6, and 24 hours. **(A-B)** Distribution of the fold change of the normalised growth (NG) with TAT-RasGAP$_{317-326}$ vs without peptide at 6 hours **(A)** and 24 hours **(B)**. The mean of the wild-type strain and the standard deviation (SD) are indicated with the vertical solid and dashed lines, respectively. Arrows indicate the strains selected as resistant, hypersensitive and more sensitive. **(C)** Growth curves of wild-type (n=270), hypersensitive (n=356) and resistant (n=20) mutants in presence or absence of 5 μM TAT-RasGAP$_{317-326}$. Data are mean ± SD. **(D)** Top 10 most represented KEGG pathways among hypersensitive strains. The number of hypersenstive strains in each pathway was normalized to the number of KEIO collection strains in the corresponding pathway. **(E)** Biological processes GO term enrichment analysis with the 10 most represented terms among the hypersensitive strains.

Figure 6. Effect of melittin, LL-37 and polymyxin B on TAT-RasGAP$_{317-326}$ activity.

(A-B) *E. coli* MG1655 was grown overnight at 37°C, diluted to OD_{600} = 0.1, and grown further during 1 hour before addition of the indicated AMPs. OD_{600} was measured at the indicated time points. For each AMP, two concentrations were tested: (A) a non-inhibitory concentration (2 μM TAT-RasGAP$_{317-326}$, 64 μg/ml melittin, 32 μg/ml LL-37 or 1 μg/ml polymyxin B) and (B) an inhibitory concentration corresponding to twice that of panel A (4 μM TAT-RasGAP$_{317-326}$, 128 μg/ml melittin, 64 μg/ml LL-37 or 2 μg/ml polymyxin B). **(C)** Combinations of AMPs were then tested and growth at 6h was expressed as percentage of growth compared to an untreated control for each combination of AMPs. **D)** Sub-inhibitory concentration of melittin interfered with TAT-RasGAP$_{317-326}$ activity. Indicated AMPs were added and OD_{600} was measured as in (A). **(E)** *E. coli* MG1655 was grown overnight at 37°C, diluted to OD_{600} = 0.1 and grown during 1 hour before addition or not of 10 μM FITC-labelled TAT-RasGAP$_{317-326}$ with or without 64 μg/ml melittin. Cells were incubated for 1 hour at 37°C, extracellular fluorescence was quenched (Intracellular) or not (Total) using 0.2% trypan blue (TB) before sample acquisition. Mean fluorescence intensities (MFI) were measured for triplicates. P values were calculated using ratio paired t-test between the indicated conditions.

Figure 7. Bacterial resistance against TAT-RasGAP$_{317-326}$ appears after selection with sub-inhibitory concentrations of peptide.

The indicated strains were incubated in presence or absence of 0.5 MIC of TAT-RasGAP$_{317-326}$. Cultures were then diluted each day in medium containing either the same concentration of the peptide or twice the concentration. Once bacterial growth was detected in the culture exposed to an elevated concentration of the peptide, the process was repeated thereby exposing the bacterial culture to sequentially increasing concentrations of peptide for a total of 20 passages. MIC of each passage was then measured and is presented as a fold change compared to the MIC of the original strain passaged in absence of peptide.

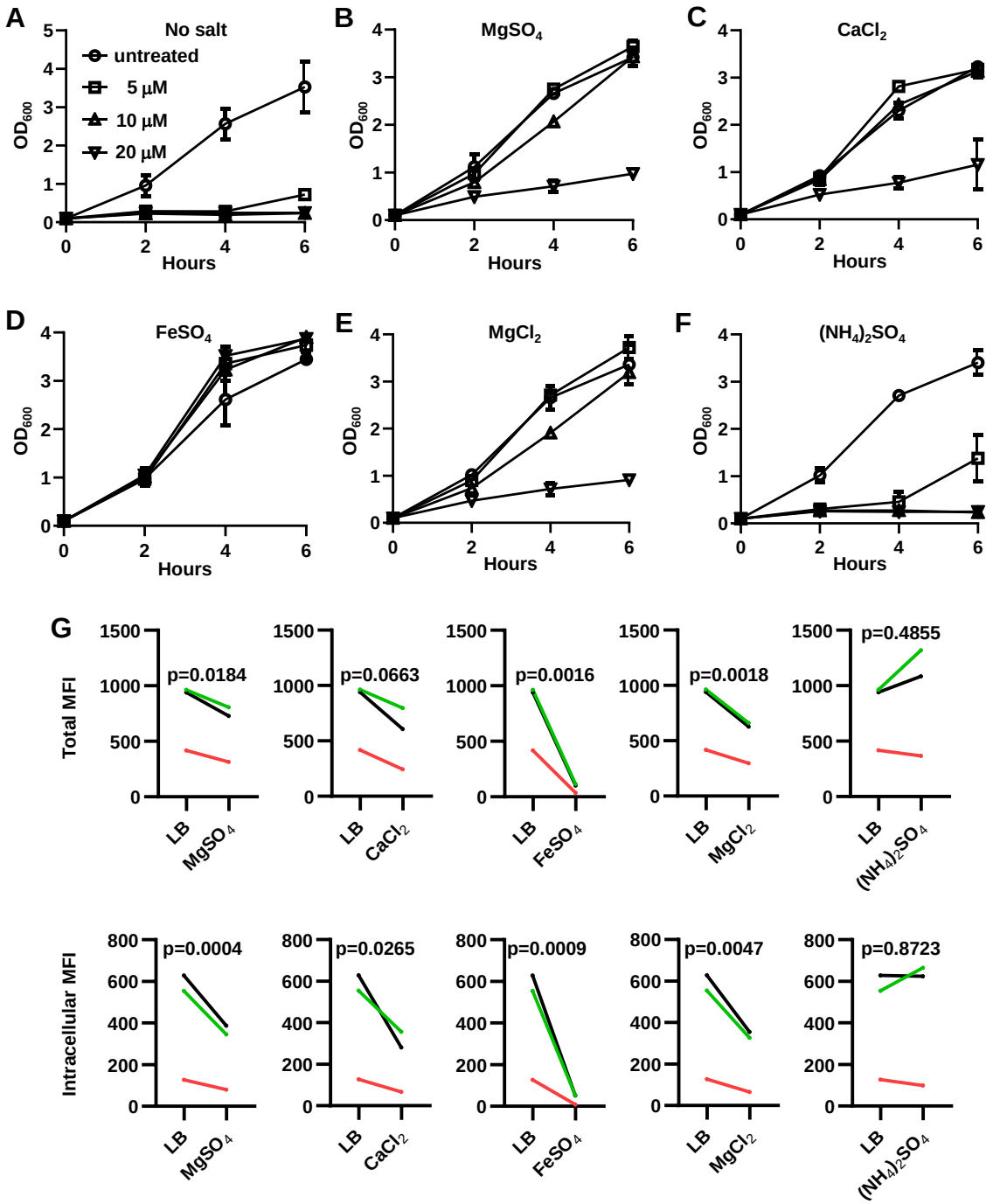

Figure 1. Divalent cations modulate bacterial resistance towards TAT-RasGAP$_{317-326}$
(A-F) *E. coli* MG1655 was grown overnight at 37°C in LB supplemented with 2 mM of the indicated salt and diluted to OD_{600} = 0.1. Bacterial suspension was then grown 1 hour at 37°C before addition of the indicated concentrations of TAT-RasGAP$_{317-326}$. OD_{600} was measured at the indicated times after the initial dilution. Error bars represent standard deviation of two independent experiments. **(G)** *E. coli* MG1655 was grown overnight at 37°C in LB containing 2 mM of the indicated salts and diluted to OD_{600} = 0.1. Bacterial binding and uptake of 10 µM FITC-labelled TAT-RasGAP$_{317-326}$ was recorded in triplicate via flow cytometry with (Intracellular) or without (Total) quenching with 0.2 % trypan blue. P values were calculated by ratio paired t-test between the indicated condition and the LB control.

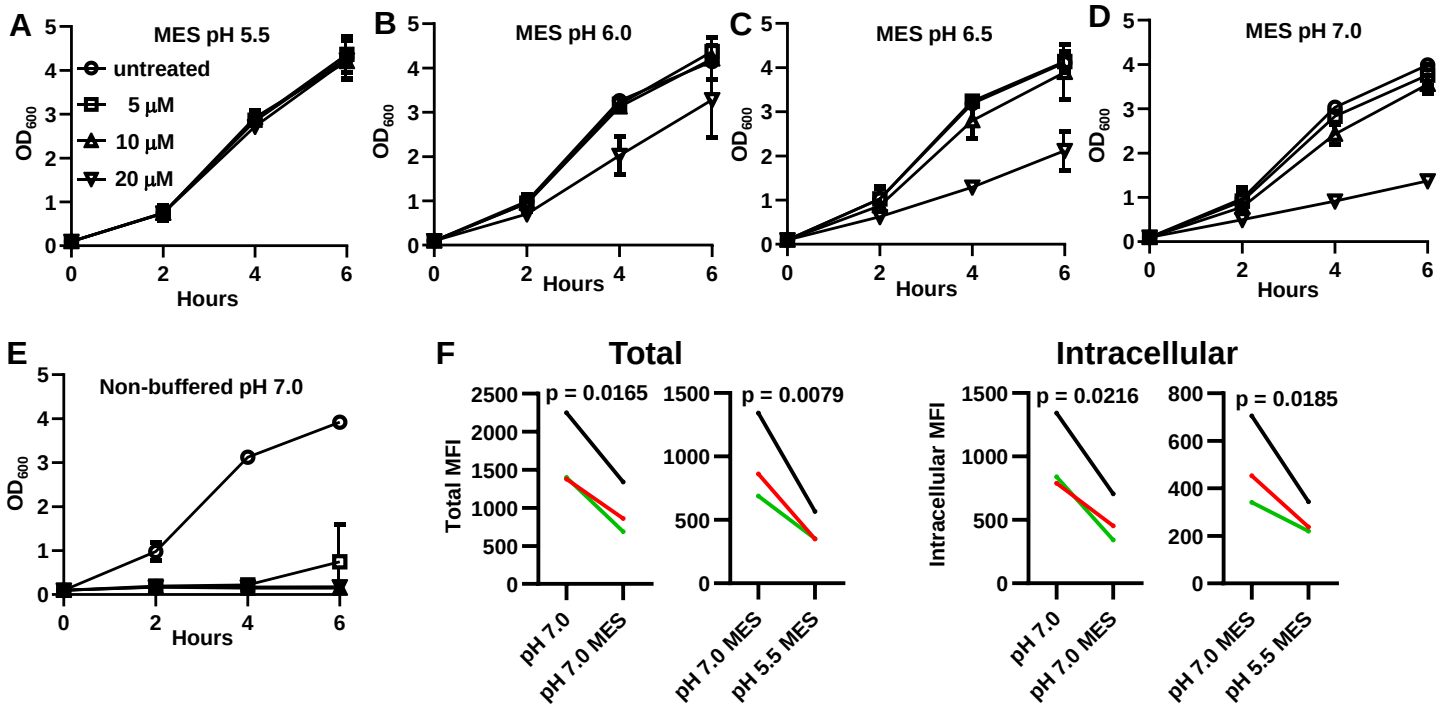

Figure 2. TAT-RasGAP$_{317\text{-}326}$ activity is negatively impacted by low pH
(A-E) *E. coli* MG1655 was grown overnight at 37°C in LB medium containing 100 mM MES at the indicated pH **(A-D)** or non-buffered LB at pH 7.0 **(E)**. Cultures were diluted to OD_{600} = 0.1 in the same medium and grown one hour at 37°C before addition of the indicated concentrations of TAT-RasGAP$_{317\text{-}326}$. OD_{600} was measured at the indicated time points. Error bars represent standard deviation of two independent experiments. **(F)** *E. coli* MG1655 was grown overnight at 37°C in LB containing or not 100 mM MES at the indicated pH, diluted to OD_{600} = 0.1 in the same medium and grown one hour at 37°C. Bacterial binding and uptake of 10 µM FITC-labelled TAT-RasGAP$_{317\text{-}326}$ was recorded in triplicate via flow cytometry with (Intracellular) or without (Total) quenching with 0.2 % trypan blue (TB). Mean fluorescence intensities (MFI) were measured for triplicates. P values were calculated using ratio paired t-test between the indicated conditions.

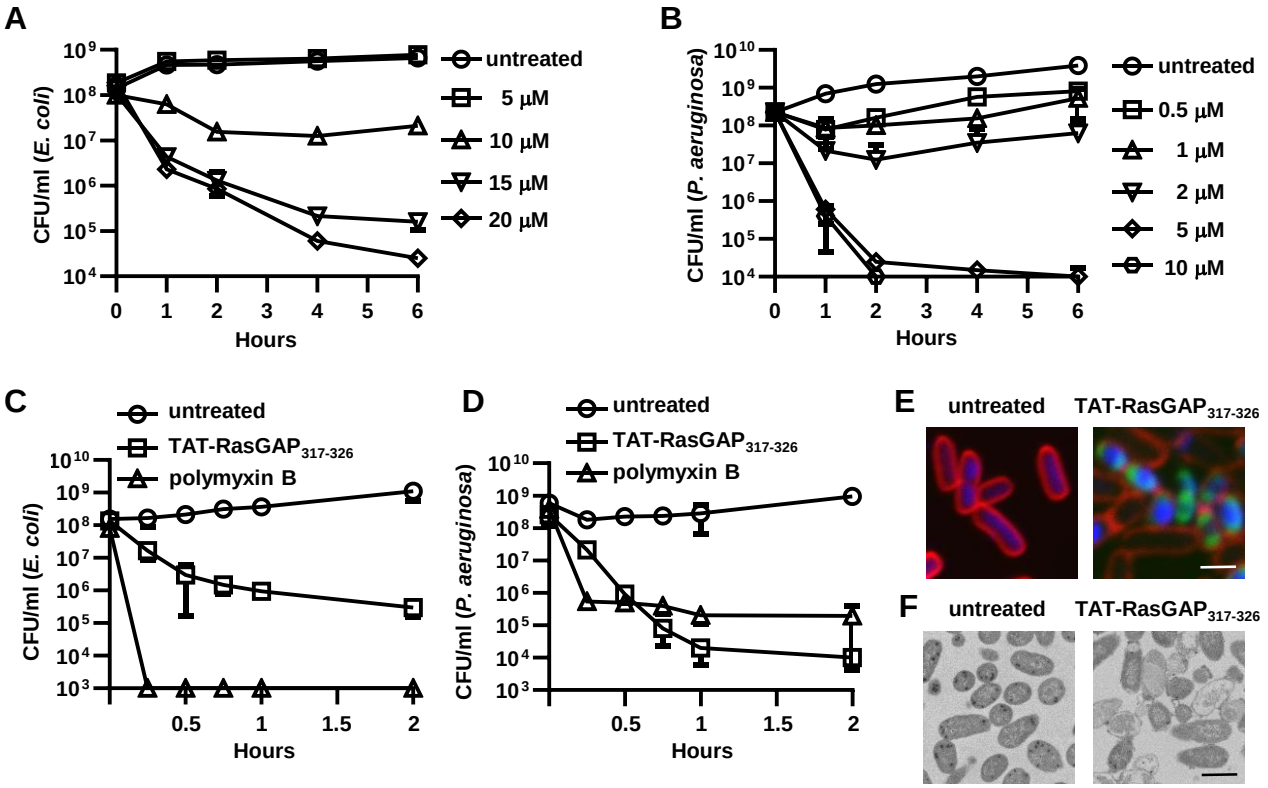

Figure 3. TAT-RasGAP$_{317-326}$ is bactericidal against *E. coli* and *P. aeruginosa*.
(A-B) Overnight cultures of *E. coli* MG1655 in LB (A) and *P. aeruginosa* PA14 in BM2 Mg^{low} (B) were diluted to OD_{600} = 0.1 and incubated at 37°C for 1 hour. TAT-RasGAP$_{317-326}$ was then added at the indicated concentrations. Samples were taken at the indicated time points, serially diluted 10-fold in fresh LB and plated on LB agar plates. Number of colony forming units per ml (CFU/ml) of original culture was calculated. Error bars show standard deviation for a minimum of two independent experiments. **(C)** *E. coli* cultures were treated as in (A). TAT-RasGAP$_{317-326}$ (20 µM) or polymyxin B (2.5 µg/ml) were added as indicated. Samples were taken at the indicated time points and CFU/ml were determined as in (A). Error bars show standard deviation of a minimum of two independent experiments. **(D)** *P. aeruginosa* cultures were treated as in (B). TAT-RasGAP$_{317-326}$ (10 µM) or polymyxin B (10 µg/ml) were added as indicated. Samples were taken at the indicated time points and CFU/ml were determined as in (A). Error bars show standard deviation of minimum of two independent experiments. **(E)** *E. coli* MG1655 grown overnight and diluted to OD_{600} = 0.1 was incubated for 1 hour with or without 10 µM FITC-labelled TAT-RasGAP$_{317-326}$ (Green). The bacteria were then labelled with 5 µg/ml FM4-64 (Red) and fixed with 4% paraformaldehyde solution. Incubation with DAPI (Blue) was subsequently performed. Pictures were taken with a Zeiss LSM710 confocal microscope and analyzed using ImageJ software. Bar = 2 µm. **(F)** *E. coli* bacteria treated for 1 hour with 10 µM TAT-RasGAP$_{317-326}$ were fixed using glutaraldehyde and prepared for electron microscopy as described in Material and Methods section. Samples were imaged via transmission electron microscopy. Images were analyzed using ImageJ software. Bar = 2 µm.

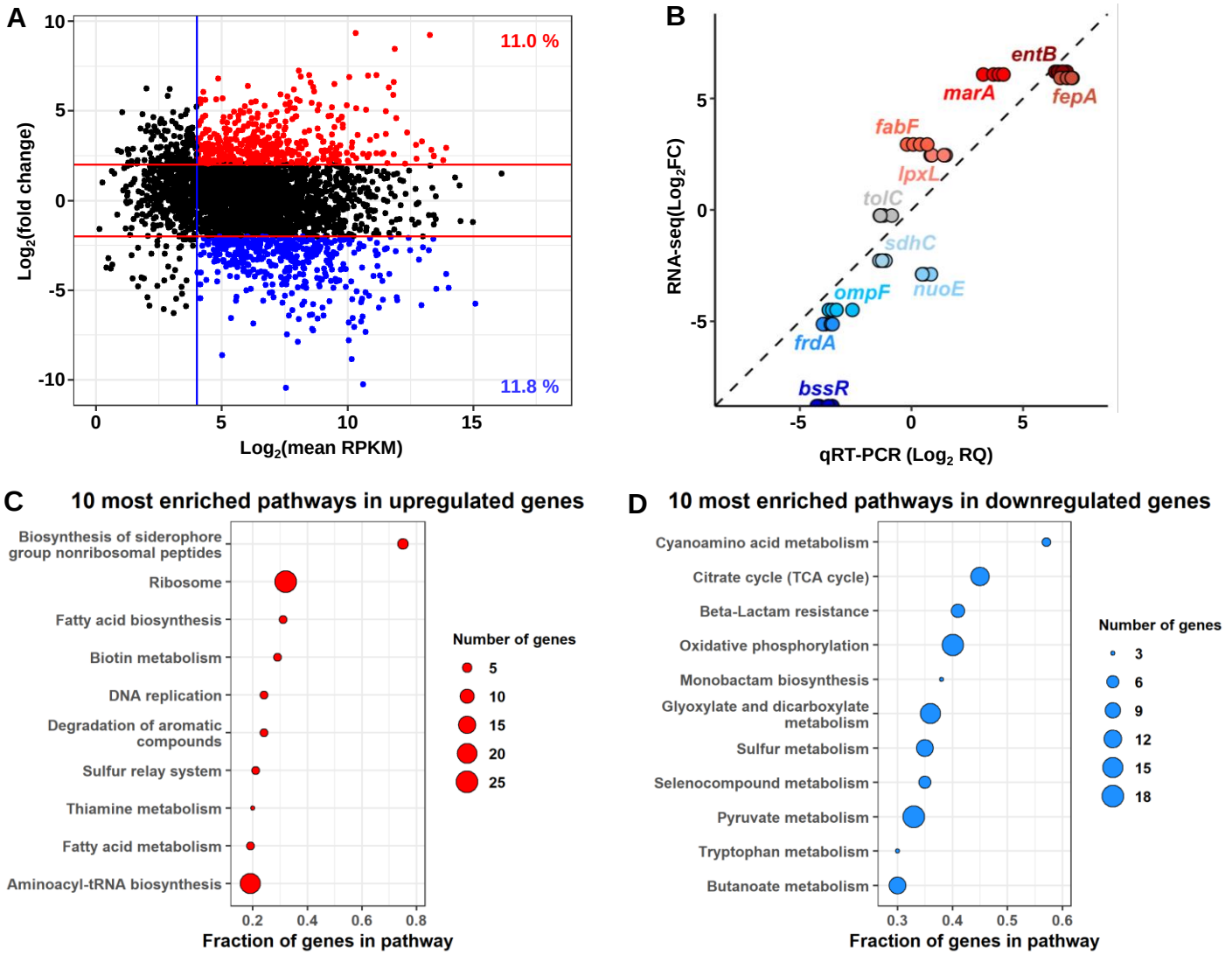

Figure 4. TAT-RasGAP$_{317-326}$ remodels the transcriptional landscape of *E. coli*.
RNA-seq analysis was performed on *E. coli* MG1655 incubated for 1 hour with or without 10 μM TAT-RasGAP$_{317-326}$. **(A)** MA-plot of the average gene expression (x-axis, RPKM: read per kilobase million) vs the differential expression (y-axis). Threshold for gene expression is indicated with the blue vertical line. The red lines indicate the cut-off limit for upregulated (red dots) and downregulated (blue dots) genes. **(B)** Correlation between RNA-seq (log_2 Fold Change) and qRT-PCR (log_2 Relative Quantification) differential expression performed on RNA extracted from *E. coli* treated for one hour with or without 10 μM TAT-RasGAP$_{317-326}$ for a set of genes detected by RNA-seq as downregulated by the peptide (blue), not changed (grey) or upregulated (red). Gene expression was measured in duplicates on two independent extracted RNA sets. **(C-D)** Fraction of KEGG pathway genes that are upregulated **(C)** or downregulated **(D)** after treatment with TAT-RasGAP$_{317-326}$. Dot size indicates the number of genes in the selection.

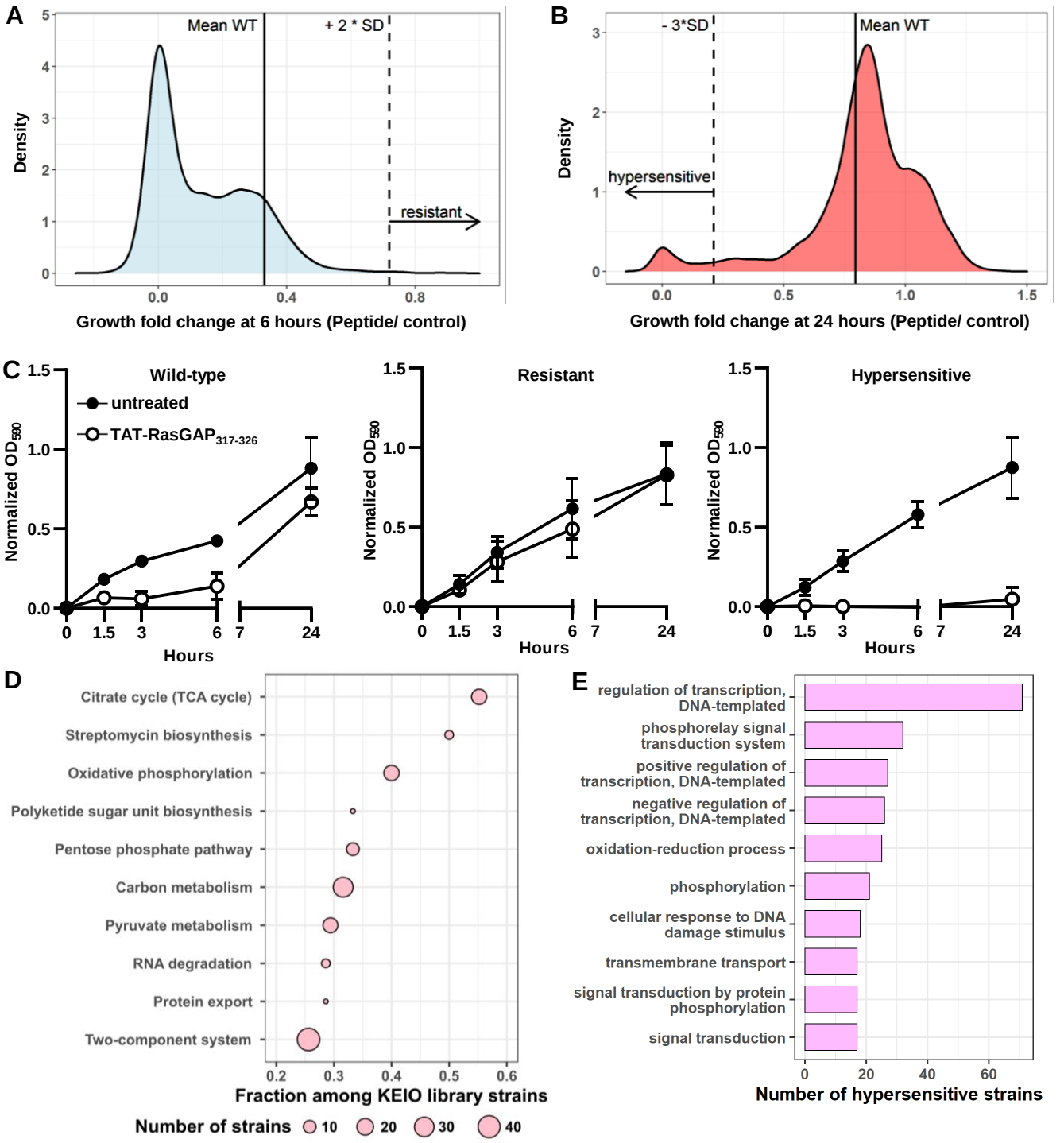

Figure 5. Selection of hypersensitive and resistant *E. coli* deletion mutants from KEIO collection. Deletion mutants and corresponding wild-type strain were grown in LB medium with or without 5 µM TAT-RasGAP$_{317-326}$ and OD$_{590}$ was measured at 0, 1.5, 3, 6, and 24 hours. **(A-B)** Distribution of the fold change of the normalised growth (NG) with TAT-RasGAP$_{317-326}$ vs without peptide at 6 hours **(A)** and 24 hours **(B)**. The mean of the wild-type strain and the standard deviation (SD) are indicated with the vertical solid and dashed lines, respectively. Arrows indicate the strains selected as resistant or hypersensitive. **(C)** Growth curves of wild-type (n=270), hypersensitive (n=356) and resistant (n=20) mutants in presence or absence of 5 µM TAT-RasGAP$_{317-326}$. Data are mean ± SD. **(D)** Top 10 most represented KEGG pathways among hypersensitive strains. The number of hypersenstive strains in each pathway was normalized to the number of KEIO collection strains in the corresponding pathway. **(E)** Biological processes GO term enrichment analysis with the 10 most represented terms among the hypersensitive strains.

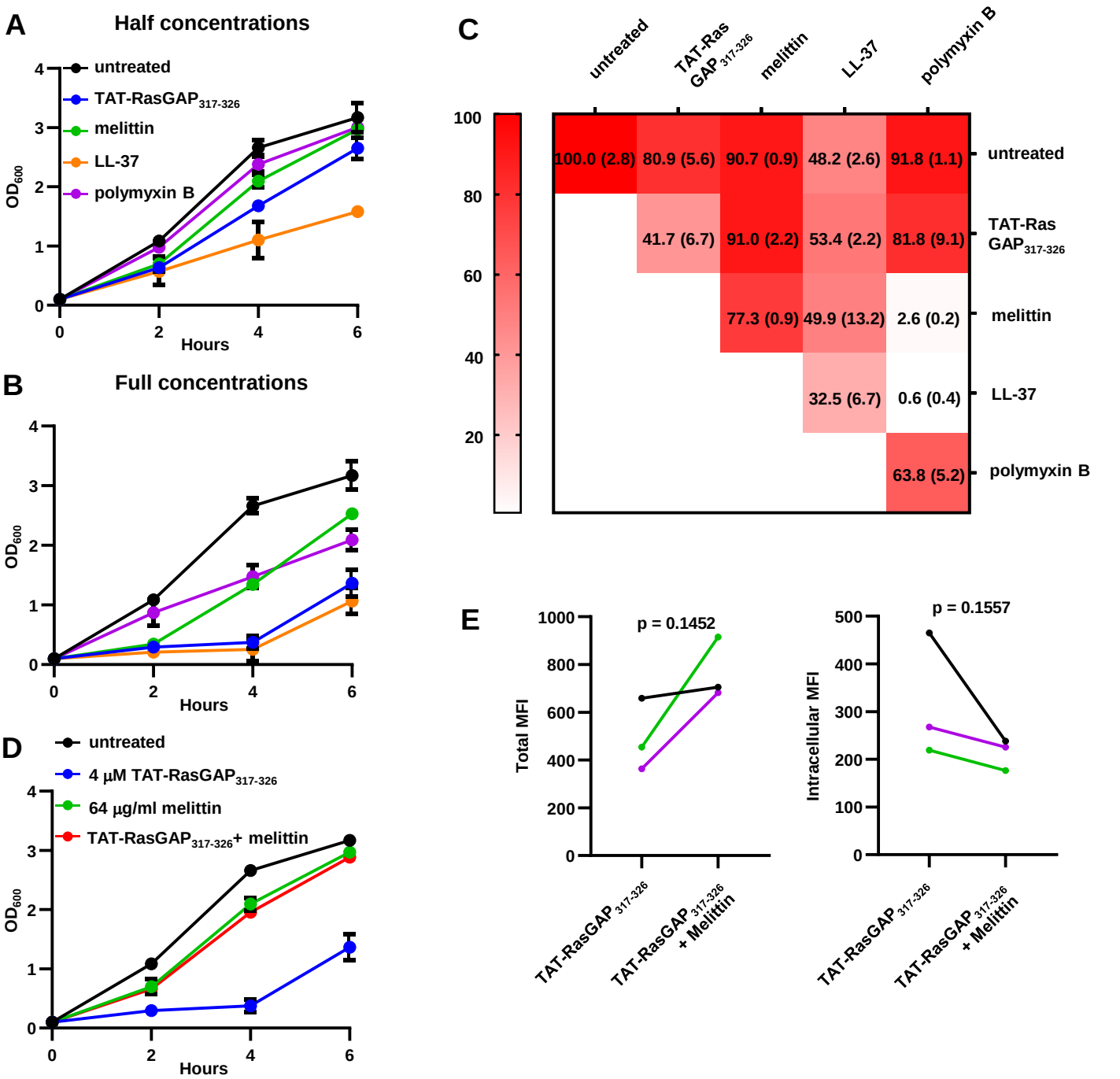

Figure 6. Effect of melittin, LL-37 and polymyxin B on TAT-RasGAP$_{317-326}$ activity.
(A-B) *E. coli* MG1655 was grown overnight at 37°C, diluted to OD_{600} = 0.1, and grown further during 1 hour before addition of the indicated AMPs. OD_{600} was measured at the indicated time points. For each AMP, two concentrations were tested: (A) a non-inhibitory concentration (2 µM TAT-RasGAP$_{317-326}$, 64 µg/ml melittin, 32 µg/ml LL-37 or 1 µg/ml polymyxin B) and (B) an inhibitory concentration corresponding to twice that of panel A (4 µM TAT-RasGAP$_{317-326}$, 128 µg/ml melittin, 64 µg/ml LL-37 or 2 µg/ml polymyxin B). **(C)** Combinations of AMPs were then tested and growth at 6h was expressed as percentage of growth compared to an untreated control for each combination of AMPs. **D)** Sub-inhibitory concentration of melittin interfered with TAT-RasGAP$_{317-326}$ activity. Indicated AMPs were added and OD_{600} was measured as in (A). **(E)** *E. coli* MG1655 was grown overnight at 37°C, diluted to OD_{600} = 0.1 and grown during 1 hour before addition or not of 10 µM FITC-labelled TAT-RasGAP$_{317-326}$ with or without 64 µg/ml melittin. Cells were incubated for 1 hour at 37°C, extracellular fluorescence was quenched (Intracellular) or not (Total) using 0.2% trypan blue (TB) before sample acquisition. Mean fluorescence intensities (MFI) were measured for triplicates. P values were calculated using ratio paired t-test between the indicated conditions.

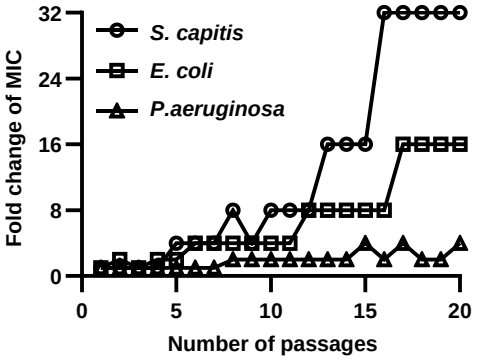

Figure 7. Bacterial resistance against TAT-RasGAP$_{317-326}$ appears after selection with sub-inhibitory concentrations of peptide.

The indicated strains were incubated in presence or absence of 0.5 MIC of TAT-RasGAP$_{317-326}$. Cultures were then diluted each day in medium containing either the same concentration of the peptide or twice the concentration. Once bacterial growth was detected in the culture exposed to an elevated concentration of the peptide, the process was repeated thereby exposing the bacterial culture to sequentially increasing concentrations of peptide for a total of 20 passages. MIC of each passage was then measured and is presented as a fold change compared to the MIC of the original strain passaged in absence of peptide.